

N 71 - 24010

**NASA TECHNICAL
MEMORANDUM**

NASA TM X-67802

NASA TM X-67802

**CASE FILE
COPY**

**IMPACT RESISTANCE OF UNIDIRECTIONAL
FIBER COMPOSITES**

by C. C. Chamis, M. P. Hanson, and T. T. Serafini
Lewis Research Center
Cleveland, Ohio

TECHNICAL PAPER proposed for presentation at
Second Conference on Composite Materials: Testing and Design
sponsored by the American Society for Testing and Materials
Anaheim, California, April 20-22, 1971

IMPACT RESISTANCE OF UNIDIRECTIONAL FIBER COMPOSITES

C. C. Chamis,¹ M. P. Hanson,¹ and T. T. Serafini²

National Aeronautics and Space Administration
Lewis Research Center
Cleveland, Ohio

ABSTRACT: Composite micromechanics and macromechanics and the miniature Izod impact test are used to investigate the impact resistance of unidirectional composites. Several composite systems are examined both theoretically and experimentally. The composites are classified theoretically relative to their impact resistance for longitudinal, transverse and shear modes. Experimental results are reported only for Izod impact with the fibers either parallel or transverse to the cantilever longitudinal axis. Impact resistance design criteria which evolved during this investigation are used to design hybrid composites with improved impact resistance. This is illustrated theoretically and demonstrated experimentally. The results show that in-situ fiber and matrix elongation-to-fracture, matrix modulus, fabrication process, fiber and void volume ratios and microresidual stresses are variables which affect the impact resistance. The ranking of composite impact resistance on the basis of measured and predicted results was in excellent agreement.

KEY WORDS: fiber composites, hybrid composites, stress analysis, structural analysis, design, impact, micromechanics, micro-residual stress, debonding, delamination, Izod impact

¹Aerospace Technologists.

²Section Head.

NOMENCLATURE

A, A_D	cross-sectional area, delaminated area, respectively
a	constant Eq. (5), superscript - averaged properties
b	width, constant Eq. (5)
c	superscript-core composite
d_f	fiber diameter
E	modulus
G	shear modulus, gravitational constant
H, h	height weight dropped, member depth
IED	impact energy density
k_f, k_{fD}, k_v	fiber volume ratio, volume ratio of pull-out fibers, void ratio
L_c, l	member length over which a uniform stress exists, length
l_{cr}, l_c	fiber debonded length, delaminated length
N_{fD}, N_{LD}	number of pull-out fibers, number of delaminated layers
P	cantilever end load
S	unidirectional composite (ply) strength: subscripts define direction and sense; superscript-shell composite
ΔT	temperature difference between composite processing and use temperatures
U	energy, strain energy
v	impacting weight velocity
W	impacting weight
x,y,z	structural axes coordinate system
1,2,3	material axes coordinate system
α	thermal coefficient of expansion

β correlation coefficients
 β_v void strain magnification on in-situ matrix
 ϵ strain: subscripts define direction and sense
 ϵ^* composite limit fracture strain
 ϕ_μ matrix strain-magnification-factor: subscripts identify strain
 σ stress: subscripts define direction
 τ shear strength for interface bond

SUBSCRIPTS

cr critical
D debonding, delamination
FPO,f fiber pull-out, fiber property
i summation index
L,l longitudinal, unidirectional composite (ply) property
m,mp matrix property, matrix limiting property
R residual stress
S shear
T tension
x,y,z directions coinciding with the structural axes
1,2,3 directions coinciding with the material axes

INTRODUCTION

An important design aspect of fiber composite structural components is their impact resistance. Some basic work on impact resistance and on other closely related properties of these materials has been reported in the literature. See for example references [1-5].³ However, the understanding of impact resistance of fiber composites has not advanced

³The italic numbers in the brackets refer to the list of references appended to this paper.

to the point where components can be designed for impact using conventional design procedures.

To obtain an insight into the impact resistance of structural components made from fiber composites we begin by examining their physical makeup. The components considered herein are made by laminating several plies; the ply is itself a unidirectional composite. A better understanding of component impact resistance can then be obtained by investigating the impact resistance of individual plies, multi-ply unidirectional composites, the interply matrix layers, and the constituent material properties and fabrication processing variables. This paper deals with such an investigation. The investigation is limited to gross-type-impact (sufficiently long impact contact times so that the entire component resists the impacting force) and to unidirectional composites which exhibit a linear static stress-strain relationship to fracture.

The objectives of the investigation are to obtain a better understanding of impact resistance through elementary theoretical considerations and simple experiments. The experiments are of a qualitative nature and serve as a means to rank the composites. The following factors are examined: interpretation of impact resistance in terms of the energy under the static stress-strain diagram; relationship of this energy to constituent material properties and fabrication processing variables; identification of prevalent failure modes; identification of constituent material properties which have a strong influence on impact resistance; construction of design criteria for improving impact resistance; and, classification of several available fiber composites on an impact resistance scale.

The theoretical expressions for predicting impact resistance are covered in the section "Theoretical Investigation." Here, impact resistance associated with single or combined fracture modes is presented and discussed. Design concepts using hybrid composites are also covered. The detailed derivations are omitted here but they are given in [6]. The experimental investigation is described in the section "Experimental Investigation." In this section, the constituent materials, fabrication process, test specimens and test methods are described. The experimental results are also discussed in this section. Both theoretical and experimental results are presented in tabular and graphical forms and can serve as an aid in design.

THEORETICAL INVESTIGATION

In general advanced unidirectional fiber composites exhibit linear stress-strain behavior (Fig. 1). Linear stress-strain relationships are also retained at high rates of loadings [7]. These linear stress strain relationships and composite micromechanics [8,9] form the basis of the theoretical development for computing the impact resistance.

The impact loadings which are considered here, are illustrated in Fig. 2. As can be seen in this figure the impact loadings are either along the material axis of the composite (longitudinal, transverse or shear) or at the free end of a cantilever.

Longitudinal Impact Resistance

Longitudinal impact loading can result in either of two modes of fracture. These are: (1) cleavage - the fracture surface consists of fractured fibers and matrix which lie approximately in the same plane. (2) Cleavage with fiber pullout - the fracture surface consists of

fractured fibers in combination with debonding and fiber pull-out. In the latter case not all of the fracture surfaces of the fibers lie on the same plane. Both of these fracture modes are extensively discussed in [3,4,10].

Impact-Induced Cleavage Fracture

The equation describing cleavage failure due to impact is obtained by determining the strain energy density. It is shown experimentally in [11] that the strain energy density correlates with Izod impact. For longitudinal impact, Fig. 1a, this is simply

$$U = \frac{1}{2} \epsilon_{\text{l11T}}^* S_{\text{l11T}} V \quad (1)$$

or

$$U = \left(S_{\text{l11T}}^2 / 2E_{\text{l11}} \right) V \quad (2)$$

where U is the strain energy, ϵ^* is the fracture strain, S is the fracture strength, E is the modulus, and V is the volume. The subscript group (l11T) is defined as follows: (l) refers to unidirectional properties (l1) identify the fiber direction and load direction in that order; (T) identifies the sense of the stress. Using composite micromechanics [9] two equations can be derived for S_{l11T} depending on whether the fibers or the matrix offer the primary resistance to fracture. The derivations are given in [6]. Here we give only the final equations. The impact resistance density (IED) of composites with E_f/E_m ratio greater than 20 is approximated by

$$\text{IED} = \frac{(1 - k_v) k_f \beta_{fT}^2 S_{fT}^2}{2E_f} \quad (3)$$

with an approximation error of less than 5 percent. The undefined vari-

ables in Eq. (3) are as follows: k_v and k_f denote void and fiber volume ratios, respectively; β_{fT} represents the in-situ fiber strength efficiency which reflects the fabrication process; the subscript f refers to fiber property. The important points to be noted in Eq. (3) are the quadratic dependence of the strain energy density on the fiber strength S_{fT}^2 and the fabrication process variable β_{fT}^2 . For a high impact resistance composite Eq. (3) imposes the following requirements: a high strength, low modulus fiber, approximately 100 percent fiber properties translation efficiency, high fiber volume ratio and low void volume ratio. Three additional points to be noted here are: (1) The dependence of the strain energy density and therefore impact resistance on S_{fT}/E_f and k_f has been clearly demonstrated in [12,13]. (2) The contribution of $(1 - k_v)\beta_{fT}^2$ is contradictory to the results predicted by the debonding and fiber pull-out mechanism. See section on debonding and fiber pull-out and also [3 and 4]. (3) Equation (3) is a simple and convenient means to rank fiber composites for longitudinal impact resistance.

A graphical representation of Eq. (3) for various available composites is shown in Fig. 3, where the strain energy density is plotted as a function of S_{fT}/E_f (fiber-strength to fiber-modulus ratio) which equals in-situ fiber elongation-to-fracture. These same composites have been ranked according to Eq. (3) in Table 1. Note in Table 1 three relatively new fibers have been listed. These are Thornel-400, HMOF (a high modulus organic fiber) and UARL-344 Glass [14].

Rank comparisons of results reported in the literature with those predicted by Eq. (3) are shown in Table 2 for notched Charpy impact, in

Table 3 for fracture toughness, and in Table 4 for energy-absorbed-to-failure at cryogenic temperatures. As can be seen in these tables, the ranking comparisons are in excellent agreement.

Effects of Micro-Residual Stresses on Impact Resistance

The contribution of the matrix to impact resistance is not negligible in composites with a strong and stiff matrix and having good interface bond. These types of composites usually have $E_f/E_m < 10$, which is typical for fiber/metallic matrix composites.

The governing equation for the impact energy density for this case is given by

$$IED = aE_{l11} \left[S_{mT} - b \frac{k_f}{E_{l11}} \right]^2 \quad (4)$$

where

$$\left. \begin{aligned} a &= \frac{1}{2} E_m^2 \\ b &= \Delta T(\alpha_f - \alpha_m)E_f E_m \end{aligned} \right\} \quad (5)$$

The subscripts l , f , and m denote ply, fiber, and matrix properties, respectively; α is the thermal coefficient of expansion and ΔT is the difference between the composite processing and use temperatures.

One very important point to be noted is Eqs. (4) and (5) is that the strain energy density depends significantly on the micro-residual stress. The micro-residual stress is represented by the parameter b in Eq. (5). This dependence has not been reported previously in the literature. It is suspected that the presence of micro-residual stress in the matrix produced some of the trends reported in [3 and 15]. However, the authors of these references did not attribute the decrease in

fracture energy to this phenomenon.

The dependence of the strain energy density and therefore the impact resistance on the micro-residual stress is illustrated in Fig. 4 for a boron-silicon carbide coated titanium system. Two sets of curves are plotted in this figure. One set is for matrix-controlled failure with and without residual stress. The other set is for fiber-controlled failure with and without residual stress. This second set was obtained from Eqs. (4) and (5) by interchanging the subscript f with m.

The important point to be noted in Fig. 4 is that impact resistance, or fracture toughness, is very sensitive to the presence of micro-residual stresses. Therefore, interpretation of experimental results from composites with $E_f/E_m < 10$ must take the micro-residual stress into account.

Longitudinal impact loadings resulting in partial cleavage failure with debonding and fiber pull-out is a combined fracture mode. This type of mode will follow the description of the single modes.

Transverse Impact Resistance

Transverse impact loadings of unidirectional composites (Fig. 2b) result in brittle fractures. The amount of energy absorbed to fracture during transverse impact is referred to as the transverse impact resistance. The strain energy divided by the volume of the material is referred to as the IED. This impact energy density as measured under the transverse stress-strain curve is shown in Fig. 1b. The governing equation is derived from the stress-strain diagram in Fig. 1b and the micromechanics relations of [9]. The governing equation for the transverse impact energy density is given by

$$I_{ED} = \frac{1}{2} \left(\beta_{22T} \frac{\epsilon_{mpT}}{\beta_v \phi_{\mu 22}} \right)^2 E_{l22} \quad (6)$$

The variables in Eq. (6) are as follows: β_{22T} is the correlation coefficient reflecting the fabrication process; ϵ_{mpT} is the maximum transverse strain that the in-situ matrix will experience when the composite is loaded in the transverse direction; β_v is the void magnification of the transverse matrix strain; $\phi_{\mu 22}$ is the matrix transverse-strain-magnification factor; and E_{l22} is the transverse composite modulus.

There are several important points to be observed in Eq. (6).

(1) The transverse impact resistance is a complex function of the fabrication process, material properties, and composite properties. (2) The degree of bond at the interface is reflected by β_{22T} , the poorer the interface bond the smaller the value for this coefficient. (3) Increases in either void or fiber content or both have inverse square effects on the transverse impact resistance. These effects result in more brittle composite behavior. (4) The impact resistance increases linearly with the transverse modulus. (5) The impact resistance increases as the square of the in-situ matrix-fracture-strain.

It is important to note that the in-situ matrix-fracture strain is not the failure strain of the bulk matrix material. For nonmetallic matrixes the former is a small fraction of the latter [9]. The difference between in-situ and bulk matrix-fracture-strain is not widely recognized. As a result, efforts to correlate theory with experiment and to develop matrix materials which would result in improved composite properties have usually failed. However both of these disparities can be remedied with suitable micromechanics models and appropriate experi-

ments [16].

The graphical representation of Eq. (6) for typical fiber composites is shown in Fig. 5. In this figure the impact energy density has been plotted as a function of fiber volume ratio. Three important points to be noted in Fig. 5 are: (1) The impact resistance of graphite fiber/epoxy is insensitive to fiber volume ratio. (2) However, boron and glass fiber/epoxy composites become quite brittle at high fiber volume ratios (greater than 0.65). (3) All fiber/nonmetallic composites have approximately the same impact resistance at about 0.50 fiber volume ratio.

The variation of the impact resistance as a function of matrix modulus is shown in Table 5 for Modmor-I/epoxy composite. As can be seen in this table, the impact resistance increases very rapidly with increasing matrix modulus. There are two reasons for this rapid increase: (1) The matrix-strain-magnification factor $\phi_{\mu 22}$ decreases rapidly while the composite transverse modulus ($E_{\perp 22}$) increases (Table 5). (2) The fiber is anisotropic, that is, the transverse fiber modulus is about 0.7 to 1.4×10^6 N/cm² (1 to 2×10^6 psi).

Shear Impact Resistance

Shear impact loadings of unidirectional composite (Fig. 2c) result in relatively brittle fracture. The amount of energy absorbed to fracture during shear impact is called herein shear impact resistance. The corresponding impact energy density as measured under the shear stress-strain curve is shown in Fig. 1c. The governing equation for shear is given by

$$IED = \frac{1}{2} \left(\frac{\beta_{12} S \epsilon_{mpS}}{\beta_v \phi_{\mu 12}} \right)^2 G_{\perp 12} \quad (7)$$

Note the similarity of Eqs. (7) and (6). Corresponding terms have analogous meanings, namely: β_{12S} , correlation factor; ϵ_{mpS} , in-situ matrix shear-fracture-strain; β_v , void contribution to the matrix shear strain; $\phi_{\mu 12}$, matrix shear-strain-magnification factor; $G_{\gamma 12}$, composite shear modulus in the plane containing the fibers.

The important points noted in discussing Eq. (6) apply to corresponding terms in Eq. (7) as well. One additional point to be noted is that Eq. (7) describes also intralaminar shear delamination as will be described subsequently.

The graphical representation for typical fiber composites is shown in Fig. 6. In this figure the IED for shear is plotted as a function of the fiber volume ratio. The important points in Fig. 6 are: (1) Boron/epoxy composites are superior in shear impact as compared with other fiber/epoxy composites when the fiber volume ratio is less than about 0.6. (2) The shear impact resistance of isotropic boron and S-glass fiber/epoxy composites is very sensitive to fiber volume ratio.

The variation of the shear IED as a function of matrix modulus for a graphite Modmor-I fiber/epoxy composite is shown in Table 5. As can be seen in this table, the shear IED increases very rapidly with increasing matrix modulus. The reason for this very rapid increase is the variation of the matrix shear-strain-magnification and the composite shear modulus (Table 5) with increasing matrix modulus. It should be noted that the shear IED increases more rapidly than the transverse IED as can be seen by comparing corresponding columns in Table 5.

Longitudinal Impact Resistance from Fiber Pull-Out

Fiber composite fractured surfaces usually exhibit some debonding

and fiber pull-out. This fracture mechanism has been investigated extensively [1-4].

Two assumptions are made to derive the governing equation. These are: (1) the energy absorbed during impact is expanded in pulling-out the fibers and (2) the interface bond strength is approximated by the intralaminar shear strength. Assumption (2) was first introduced in Ref. 2. The detailed derivations leading to the governing equation are given in [6]. The result for the impact energy density from fiber pull-out is given by

$$\text{IED} = \frac{1}{8} (1 - k_v) \left(\frac{\beta_v \phi_{\mu 12}}{\beta_{12} S_{mpS}^{\epsilon}} \right) \frac{S_f^2 T}{G_{\gamma 12}} \quad (8)$$

The symbols in Eq. (9) have been defined previously. Equation (8) describes IED due to fiber pull-out as a complex function depending on: fabrication process, fiber and void contents, constituent strength properties, and composite shear modulus. The variation of IED as a function of constituent elastic properties is not easily seen in Eq. (8) because the parameter $(\phi_{\mu 12}/G_{\gamma 12})$ depends on fiber and void contents, and on the constituent properties in a complex way. This parameter is defined herein as the "Debonding Parameter" because it is an indication of the local interface shear bond. Its dependence on matrix modulus and fiber volume ratio is shown in Fig. 7 for Modmor-I fiber/epoxy composites. Note the scales in this figure. The leaders from the curves point to the corresponding scales. For example the dependence of the $(\phi_{\mu 12}/G_{\gamma 12})$ on fiber volume ratio is represented by the upper curve with $(\phi_{\mu 12}/G_{\gamma 12})$ plotted on the right against k_f on the top.

The important points to be noted from Eq. (8) in conjunction with Fig. 7 are: (1) Local bonding is enhanced with increasing fiber volume ration (up to about 0.65) or increasing matrix modulus. (2) Impact energy density (IED) due to debonding can be increased by any or combinations of the following: poor interface bond, low in-situ matrix elongation-to-failure, large (G_{f12}/G_{m12}) ratio; and constituent selection which result in low shear modulus (G_{z12}) composition.

It is important to note that the parameters which enhance IED from debonding and fiber pull-out are quite detrimental to composite structural integrity with respect to strength and stiffness.

Impact Resistance Due to Delamination

Delamination in the context used here refers to the delamination due to shear of interply layers in multilayered composites. The energy expended is referred to herein as the "impact resistance due to delamination."

The governing equation to describe this resistance is based on the following assumptions: (1) Delamination occurs when the interlaminar shear strength has been exceeded. (2) Several interply layers could delaminate simultaneously. The detailed derivations are given in [6]. The resulting equation for the impact energy density from delamination is given by

$$\text{IED} = \frac{1}{2} N_{LD} \left(\frac{\beta_{12} \epsilon_{mpS}}{\beta_v \phi_{\mu 12}} \right)^2 G_{z12} \quad (9)$$

where N_{LD} is the number of delaminated interply layers and all other symbols have been previously defined.

Note that Eq. (9) is identical with Eq. (7) except for the coeffi-

cient N_{LD} . Therefore, the discussion following Eq. (7) and the important points noted there apply to Eq. (9) as well.

The additional point to be noted from Eq. (9) is, that for improved impact resistance, design the part to assure multi interply delamination. This should be applicable to high velocity impact as well as low.

Longitudinal Impact with Cleavage and Fiber Pull-Out

This type of impact resistance results in fractured surfaces consisting of broken fibers with debonding and fiber pull-out. It was referred to as cleavage with debonding previously. The governing equation is a combination of Eqs. (3) and (8). The result for the impact energy density for this case is given by

$$IED = (1 - k_v) \frac{s_{fT}^2}{2E_f} \left[\beta_{fT}^2 k_f + \frac{d_f k_{fD}}{4 L_c} \left(\frac{\beta_v \phi_{\mu 12}}{\beta_{12} s_{mpS}} \right) \frac{E_f}{G_{12}} \right] \quad (10)$$

where L_c is the length of the component subjected to uniform stress which cause fiber fracture. The other parameters in Eq. (10) have been previously defined.

It is important to note that the fiber pull-out contribution (second term in Eq. (10)) to impact resistance in Eq. (10) is strongly dependent on L_c . The following example will illustrate the point: Using typical values for Modmor-I fiber/matrix composite and assuming 40 percent fiber pull-out, the contribution is approximately $0.3/L_c$. This contribution is negligible for longitudinal impact where L_c is quite large. However, the fiber pull-out contribution will be significant in the case of localized or bending impact.

The fiber pull-out contribution will, in general, be negligible (less than about 1 to 2 percent) if

$$\left(\frac{d_f}{L_c}\right) \left(\frac{E_f}{G_{l12}}\right) < 10^{-5} \quad (11)$$

Equation (10) indicates that composites with high modulus and low intralaminar shear strength are good candidates for high impact resistance. Since Eq. (10) is a combination of Eqs. (3) and (8) the discussion following these equations applies to Eq. (10) as well.

HYBRID COMPOSITES TAILOR-MADE FOR IMPROVED IMPACT RESISTANCE

Hybrid composite is the term used for a composite which consists of two or more different fiber matrix combinations. Typical examples are: Modmor-I/epoxy-Glass/epoxy-Modmor-I/epoxy; HTS/epoxy-Thornel-50/epoxy-HTS/epoxy and others.

Using these composites for improved impact resistance is a major contribution of this investigation. The concept was discovered during the experimental portion of the investigation. It was observed that some of the impacted cantilever specimens exhibited combined fracture modes consisting of fiber breakage, fiber pull-out and interply delamination.

The hybrid composite takes advantage of two or more of these modes to improve impact resistance. It is an important and useful concept in designing structural components in general. The impact resistance of hybrid composites is thus not a material characteristic.

The concept is illustrated here, by applying it to the cantilever structure shown in Fig. 8. The governing equation for impact energy density is given by

$$I_{ED} = \frac{1}{2} \frac{S_{l11T}^s}{E_{l11}^s} \left\{ \left[\frac{1}{9} + \frac{1}{30} \left(\frac{h}{l} \right)^2 \left(\frac{E_{l11}^a}{G_{l12}^a} \right) \right] + \frac{1}{16N_{LD}} \left(\frac{h}{l} \right) \frac{E_{l11}^s}{S_{l12}^c} \right. \\ \left. + \frac{\pi}{16} \left(\frac{N_{fD} d_f^3}{bh l} \right) \left(\frac{E_{l11}^s}{S_{l12}^s} \right) \left(\frac{S_{fT}^s}{S_{l11T}^s} \right)^2 \right\} \quad (12)$$

The undefined notation in Eq. (12) is as follows: the superscripts (a), (s), and (c) represent averaged core-shell, shell and core, respectively. The subscript (1) refers to unidirectional composite properties along the direction indicated by the numerical subscripts following (l). The variables b, h, and l represent width, depth, and length of the cantilever, respectively. See also Fig. 8. The variables d_f , N_{fD} , and N_{LD} represent fiber diameter, number of fibers that pulled out, and number of layers that delaminated, respectively.

Examining Eq. (12) reveals that the shear contribution depends on E_{l11}^a/G_{l12}^a and both fiber pull-out and delamination depend on the parameter E_{l11}/G_{l12} . This means that in order to take advantage of the high shear contribution of, fiber pull-out and/or delamination, high longitudinal modulus, low shear modulus and low intralaminar strength composites should be selected. Some composites which meet this criterion are Thorne1-50, Modmor-I, and HMOF fibers in a resin matrix.

There are three other sets of parameters in Eq. (12) which need careful examination in designing hybrid composites for improved impact resistance. These are: (1) $(h/l)^2$ - for the shear contribution; (2) $(h/N_{LD} l)$ - for delamination; and (3) $(d_f^3 N_{fD} / bh l)$ - for fiber pull-out.

The shear contribution will be greater than 3 percent when

$$(l/h)^2 > 10 \frac{E_{\tau 11}^a}{G_{\tau 12}^a} \quad (13)$$

The contribution of the fiber pull-out will be greater than 3 percent

when

$$\left(\frac{d_f^3 N_{FD}}{bh^2} \right) > 0.02 \left(\frac{s_{\tau 12S}^c}{E_{\tau 11}^s} \right) \quad (14)$$

The contribution of the delamination will be greater than 3 percent when

$$\left(\frac{h}{N_{LD} l} \right) > 0.06 \left(\frac{s_{\tau 12S}^c}{E_{\tau 11}^s} \right) \quad (15)$$

The inequality

$$s_{\tau 12S}^c \leq \frac{1}{4} \left(\frac{h}{l} \right) \text{MIN} \left(s_{\tau 11T}^s, s_{\tau 11C}^s \right) \quad (16)$$

must be satisfied for delamination. The variable $s_{\tau 11C}^s$ denotes longitudinal compressive strength.

Equation (12) in conjunction with the inequalities Eqs. (13-16) and provide relations which can be used to select parameters in designing composites with improved impact resistance. They were used in this investigation to guide the selection of the hybrid composites.

The inequalities Eqs. (13-16) can be expressed in terms of constituent properties by using the micromechanics relations for $s_{\tau 11T}$, $s_{\tau 11C}$, $s_{\tau 12S}$, and $E_{\tau 11}$.

EXPERIMENTAL INVESTIGATION

This portion of the investigation consisted of carrying out miniature-Izod [17] impact tests to verify qualitatively the theoretical considerations and concepts described in the "Theoretical Investigation" Section.

Materials and Specimen Fabrication

Graphite, glass and HMOF fibers in an epoxy resin matrix were used in the experimental investigation. The various fibers are listed in Table 6. All fiber material was drum wound and impregnated with the epoxy resin ERL 2256-ZZL0820 (27.0 pph resin).

Composites were fabricated by means of a unidirectional lay-up of a number of "B" staged plies to yield the thickness desired. Most of the composites consisted of fibers of one particular type. Some hybrid composites were also fabricated that consisted of two fiber types in the lay-up with selected thickness and position of each. The composites were cured under heat and pressure in a matched-die mold. Complete curing conditions are included in Table 6.

Miniature Izod specimens were machined from the fabricated composites in both the longitudinal and transverse directions. The finished specimen dimensions were $7.9 \times 7.9 \times 37.6$ mm.

Test Apparatus and Procedure

The impact machine used was a modified Bell Telephone Laboratory pendulum type (Fig. 9). The design capacity of the pendulum was 240 centimeter-Newtons (27 inch-pounds). Addition of weights to the pendulum increased the capacity to 1010 centimeter-Newtons (114 inch-pounds). The striking velocity of the pendulum was 345 cm per second. The Izod specimens were struck at their free end, 22 mm from the edge of the grip. The specimen length in the grip was 14 mm. A "dead weight" load was applied to the grip to assure uniform gripping of specimens.

Composites of one particular fiber were tested in both the longitudinal and transverse directions. Hybrid composites were generally

tested in the longitudinal direction with the plies parallel to the striking pendulum. The angular displacement of the pendulum after impact was an inverse measure of the impact energy. Typical fractured specimens from this method of testing are shown in Fig. 10.

EXPERIMENTAL RESULTS AND DISCUSSION

Longitudinal and Transverse Impact

Several specimens of each composite system were tested in longitudinal and transverse impact. Also specimens from the matrix system were tested. The results are presented in Bar-Graph form in Fig. 11. The adjacent bars have the following meaning: the left bar denotes longitudinal while the right denotes transverse impact. The scatter is indicated by the light lines within the bar.

Photomicrographs of typical fracture surfaces are shown in Fig. 12. Note the fracture modes, cleavage, and cleavage with fiber pull-out. Photographs of fractured specimens are shown in Fig. 10. Impact resistance versus short-beam intralaminar shear strengths for several of these composites are given in Fig. 13. The intralaminar shear strengths are needed to assist with the theoretical impact resistance ranking of the test specimens.

Measured results of longitudinal impact normal and parallel to the lamination directions were identical. This is to be expected in unidirectional composites with nonmetallic matrices.

Discussion of Experimental Results and Comparison of Ranking

Examination of Figs. 10 and 11 reveal that: (1) Those composites which exhibit more than one fracture mode have higher impact resistance in general. (2) Composite transverse impact results in brittle fracture

and the value is considerably lower than that of the matrix. Some fiber splitting occurs in the Thornel fiber composites. (3) The hybrid composite experienced two or more fracture modes.

Averaged values of the experimental results are summarized in Table 6. The last two columns of this table contain the ranking with respect to impact resistance. The numbers enclosed in circles in these columns represent the ranking of the measured values. The numbers enclosed in squares represent the predicted ranking. As can be seen, the ranking is identical. The predicted ranking was obtained as follows: For the longitudinal ranking, Eq. (13) was used in conjunction with Table 1 and Fig. 13. For the transverse ranking Eq. (6) was used in conjunction with Fig. 13. The use of Fig. 13 for the transverse strength is acceptable because both intralaminar shear and transverse composite strengths exhibit similar trends.

It is interesting to note in Table 6 that one of the hybrid composites (HTS/T505/HTS) had larger impact resistance than either of the two constituent composites. The explanation is that the hybrid composite had more delaminated surfaces. This, of course, is the essence of the hybrid composite concept for improved impact resistance.

The important point to keep in mind from this discussion is that theoretical expressions can be constructed to predict impact resistance at least on a qualitative basis. These expressions can be used to guide research for constituent materials and design concepts for improved impact resistance.

CONCLUSIONS

Results from this investigation of gross-type-impacts of composites

involving relatively long impact contact times lead to the following conclusions:

1. The impact resistance of unidirectional composites is ranked using elementary composite mechanics and criteria are presented to guide design for improved resistance.
2. Theoretical results show that in composites with high fiber-to-matrix modulus ratios, the longitudinal impact resistance is fiber controlled. When this ratio is twenty, the matrix contribution is less than 5 percent. However, the transverse and shear impact resistances are matrix controlled.
3. Theoretical results show that in composites with fiber-to-matrix modulus or strength ratios about four, the longitudinal impact resistance could be matrix controlled. In this case, the presence of micro-residual stresses decreases the impact resistance considerably.
4. Theoretical considerations indicate that the impact resistance can be improved by designing the composite so that fiber breaks, fiber debonding with fiber pull-out and partial delamination take place at the same time. Any combinations of these fracture modes will also improve the impact resistance.
5. Theoretical considerations also show that the impact resistance is sensitive to void and fiber contents and to certain fabrication factors which are reflected in the in-situ constituent properties.
6. The experimental results indicate three prevalent longitudinal failure modes due to impact. These are cleavage, cleavage with some fiber pull-out, and cleavage combined with partial delamination due to intralaminar shear failure.

7. The transverse failure mode was cleavage. The fracture surface included matrix fracture, fiber debonding, and some fiber splitting. The experimental results showed that the impact resistance was the same whether the specimen was impacted parallel or normal to the lamination direction.

8. Ranking of predicted results was in good agreement with that of measured results from notched Charpy Impact, cryogenic fracture toughness, stress intensity, and unnotched Izod impact.

9. The hybrid composite concept is an efficient composite design to combine high strength and high stiffness with high impact resistance.

REFERENCES

- [1] Tetelman, A. S., "Fracture Processes in Fiber Composite Materials," Adhesion, ASTM STP 460, Composite Materials: Testing and Design, ASTM STP 460, Am. Soc. Testing Mats., 1969, p.540, p. 473.
- [2] Novak, R. E., "Fracture in Graphite Filament Reinforced Epoxy Loaded in Shear," Composite Materials: Testing and Design, ASTM STP 460, Am. Soc. Testing Mats., 1969, p. 540.
- [3] Kelly, A., "Interface Effects and the Work of Fracture of a Fibrous Composite," NPL-IMS-10, National Physical Lab., Feb. 1970.
- [4] Outwater, J. O. and Murphy, M. C., "Fracture Energy of Unidirectional Laminates," Modern Plastics, Vol. 47, Sept. 1970, p. 160.
- [5] Rotem, A. and Lifshitz, J. M., "Longitudinal Strength of Unidirectional Fibrous Composite Under High Rate of Loading," 26th Annual SPI Conference, 1971, Sec. 10-G.
- [6] Chamis, C. C., Hanson, M. P. and Serafini, T. T., "Designing for Impact Resistance with Unidirectional Fiber Composites," Proposed NASA Technical Note, Nat. Aeronautics and Space Administration.

- [7] Chiao, T. T. and Moore, R. L., "Stress-Rupture of S-Glass/Epoxy Multi-filament Strands," Journal of Composite Materials, Vol. 5, 1971, p. 2.
- [8] Chamis, C. C., "Thermoelastic Properties of Unidirectional Filamentary Composites by a Semiempirical Micromechanics Theory," Science of Advanced Materials and Process Engineering, Vol. 14, Western Periodicals Company, 1968, Paper I-4-5.
- [9] Chamis, C. C., "Failure Criteria for Filamentary Composites," NASA TN D-5367, Nat. Aeronautics and Space Administration, 1969.
- [10] Daniel, I. M., "Photoelastic Study of Crack Propagation in Composite Models," Journal of Composite Materials, Vol. 4, 1970, p. 178.
- [11] Broutman, L. J. and Sahu, S., "The Effect of Interfacial Bonding on the Toughness of Glass Filled Polymers," 26th Annual SPI Conference, 1971, Sect. 14-C.
- [12] McGarry, F. J. and Mandell, J. F., "Fracture Toughness of Fiber Reinforced Composites," Research Report R70-79, Massachusetts Inst. Tech., Dec. 1970.
- [13] Aulenbach, T. H., et al., "Fracture Toughness Testing of Fibrous Glass Resin Composites," presented at the 25th SPI Annual Conference, Washington, D.C., Feb. 6-9, 1970.
- [14] Bacon, J. F., "Investigation of the Kinetics of Crystallization of Several High Temperature Glass Systems," Rep. J910939-3, United Aircraft Research Lab., Sept. 1970.
- [15] Cooper, R. E., "The Work-To-Fracture of Brittle-Fibre Ductile-Matrix Composites," Journal of the Mechanics and Physics of Solids, Vol. 8, 1970, p. 179.

- [16] Patsis, A. V., et al., "Correlation of Graphite-Fiber/Epoxy Composite Strength with Matrix Tensile Properties," Proposed NASA Technical Note, Nat. Aeronautics and Space Administration.
- [17] Compton, W. A., and Steward, K. P., "Test Specifications Manual Composite Materials For Turbine Compressors," AFML-TR-68-31, Pt. II, Solar Div., International Harvester, Apr. 1968.
- [18] Alfring, R. and Simon, R. A., "Properties of Graphite Fiber Composites at Cryogenic Temperatures," NOLTR-69-183, NASA-CR-72652, Naval Ordnance Lab., May 1970.
- [19] Chamis, C. C., "Computer Code for the Analysis of Multilayered Fiber Composites - Users Manual," NASA TN D-7013, Nat. Aeronautics and Space Administration, 1971.

TABLE 1. - LONGITUDINAL IMPACT RESISTANCE OF VARIOUS FIBER/RESIN MATRIX COMPOSITES

 $(k_f = 0.5, k_v = 0, \text{ AND } \beta_{fT} = 1.0)$

Fiber	Density cm/cm ³	Density lb/in. ³	Fiber modulus 10 ⁵ N/cm ²	Fiber modulus mpsi	Fiber strength 10 ⁵ N/cm ²	Fiber strength ksi	Predicted longitudinal impact energy density cm-N/cm ³	Predicted longitudinal impact energy density lb-in./in. ³	Rank
Boron	2.62	0.095	414	60	3.18	460	608	880	7
E-glass	2.49	.090	69	10	2.58	360	2240	3250	3
S-glass	2.49	.090	86	12.4	4.62	670	6250	9050	1
Modmor-I	1.99	.072	414	60	1.73	250	179	260	10
Modmor-II	1.74	.063	262	38	2.52	350	656	950	6
Thornel-400	1.71	.062	207	30	2.90	420	1020	1470	5
Thornel-50	1.63	.059	345	50	1.66	240	200	290	9
Thornel-75	1.85	.067	473	75	2.62	380	324	470	8
HMOF	1.38	.050	173	25	2.76	400	1040	1600	4
UARL-344 glass	3.60	.130	128	18.6	4.83	700	4860	7050	2

TABLE 2. - COMPARISON OF PREDICTED RESULTS WITH NOTCHED CHARPY IMPACT DATA (REF. 13)
WITH FIBERS PARALLEL TO THE LONGITUDINAL AXIS OF THE BEAM

Composite	Fiber volume ratio	10^5 N/cm^2	Fiber modulus 10^5 N/cm^2	Fiber strength 10^5 N/cm^2	Measured (Ref. 13)			Predicted ($k_v = 0; \beta_{FT} = 1.0$)			Impact energy in.-lb/in.	Rank
					cm-N	ft-lb	Rank	cm-N/cm	in.-lb/in.			
Thornel-50/epoxy	0.55	345	50	1.66	240	544	4	218	315		4	
Boron/epoxy	.55	404	58.5	3.18	460	1356	10	3	687	995	3	
UARL-344 glass/ epoxy	.633	128	18.6	4.83	700	4080	30	2	5760	8 350	2	
S-glass/epoxy	.65	85.5	12.4	4.62	670	7340	54	1	8160	11 800	1	

TABLE 3. - COMPARISON OF IMPACT ENERGY DENSITY WITH MEASURED
FRACTURE TOUGHNESS FOR GLASS-FABRIC COMPOSITES

Specimen	Results from Table 6, Ref. 11			Predicted IED ^b			
	Fiber volume ratio	Measured fracture toughness, K_{IC}^a	(ksi-in. ^{1/2})	K_{IC}	$N\text{-cm}/cm^3$	1b-in./in. ²	Rank
1-18	0.545	27.2-28.8	24.8-26.2	3	1700	2460	3
2-18	.476	22.4-25.0	20.4-22.7	4	1460	2120	4
3-18	.589	40.8-41.8	37.2-38.1	2	1830	2650	2
4-18	.676	43.1-46.8	39.2-41.7	1	2110	3050	1
5-18	.294	17.4-20.6	15.8-18.7	5	912	1320	5
6-18	.225	16.4-18.0	14.9-16.4	6	701	1015	6

^aResults were obtained from bending tests.

^b $S_{FT} = 207 \text{ N/cm}^2$ (300 ksi); $E_F = 6.9 \times 10^6 \text{ N/cm}^2$ (10×10^6 psi); $k_v = 0$; $\beta_{FT} = 1.0$.

TABLE 4. - COMPARISON OF IMPACT ENERGY DENSITY WITH MEASURED DATA OF GRAPHITE FIBER/EPOXY COMPOSITES AT CRYOGENIC TEMPERATURES

[T = 20.3 R (-423° F), Ref. 20]

Matrix type Measured ^a cm-N/ cm ²	Fiber volume ratio	Rank	Fiber modulus ^b 10 ⁵ N/cm ²	Fiber strength ^b 10 ⁵ N/cm ²	ksi	Measured ^a cm-N/ cm ²	in.-lb/ in. ²	Rank	Composite fracture energy cm-N/ cm ³	in.-lb/ in. ³	Rank		
7.3	10.6	3	0.38	324	47	1.59	230	46	67	4	148	214	4
7.1	10.4	4	.39	338	49	1.64	238	29	42	5	155	225	3
2.9	4.2	6	.40	345	50	2.54	368	152	220	1	372	540	1
8.2	11.9	2	.40	297	43	2.68	289	64	93	2	279	390	2
8.5	12.3	1	.42	332	48	1.50	218	58	84	3	144	208	5
3.4	5.0	5	.41	311	45	.99	143	23	33	6	64	93	6

^aMeasured by the beam splitting method (Ref. 20).

^bReported in Ref. 20.

TABLE 5. - EFFECTS OF MATRIX MODULUS ON TRANSVERSE AND SHEAR IMPACT

ENERGY DENSITY (MODMOR-I/EPOXY; $k_f = 0.5$, $k_v = 0$)

Matrix modulus 10^5 N/cm^2	Strain magnifi- cation factors ^a	Unidirectional composite modulus ^a			Predicted impact energy density		
		Transverse	Shear	10^5 N/cm^2	10^5 N/cm^2	Transverse	Shear
0.69	0.1	3.26	4.37	1.86	0.27	0.97	0.14
2.07	.3	1.96	3.54	4.35	.63	2.56	.37
3.45	.5	1.42	2.97	5.86	.85	3.80	.55
4.82	.7	1.12	2.56	6.89	1.00	5.18	.75
6.89	1.0	1.00	2.12	7.95	1.15	6.14	.89
10.03	1.5	1.00	1.65	9.05	1.31	7.66	1.11

^aThe value in these columns was generated with the computer code of Ref. 18.

TABLE 6. - MINIATURIZED IZOD IMPACT DATA FOR FIBER-EPOXY^(a) COMPOSITES

Fiber	Type	Surface treatment	Fiber volume ratio	Fiber direction	Average impact energy cm-N in.-lb	Ranking ^e Long. Trans.
Graphite	T505	(b)	0.532	Long.	85.9 7.6	⑤ [5] ③ [3]
				Trans.	7.9 0.7	
Graphite	T50	Polyvinyl alcohol	0.583	Long.	208.0 18.4	④ [4] ⑤ [5]
				Trans.	3.4 0.3	
Graphite	HTS	(c)	0.523	Long.	56.5 5.0	⑥ [6] ② [2]
				Trans.	14.7 1.3	
Graphite	MI	None	0.542	Long.	215.0 19.0	③ [3] ④ [4]
				Trans.	4.5 0.4	
Glass	S	(d)	0.486	Long.	757.0 67.0	① [1] ① 1
				Trans.	15.8 1.4	
HMOF		---	---	Long.	280.0 24.8	② [2] ⑤
				Trans.	3.4 0.3	
Graphite	HTS		0.598	Long.	116.3 10.3	3
				Trans.	11.3 1.0	
Graphite	HMS		0.536	Long.	132.0 11.7	2
Graphite	HMS		---	Long.	232.0 20.5	1

^aEpoxy resin - ERL 2256/AAL 0820, Union Carbide Corp. "B" stage of impregnated fiber - 93° C, 45 min. Mylar cover, cure cycle - under 50 psi pressure, 2 hrs - 82° C, 3 hrs - 148° C.

^bEpoxy compatible - Union Carbide Corp.

^cHeat cleaned - Hercules Corp.

^d901 - Owens Corning Fiberglas Co.

^e Measured rank, Predicted rank.

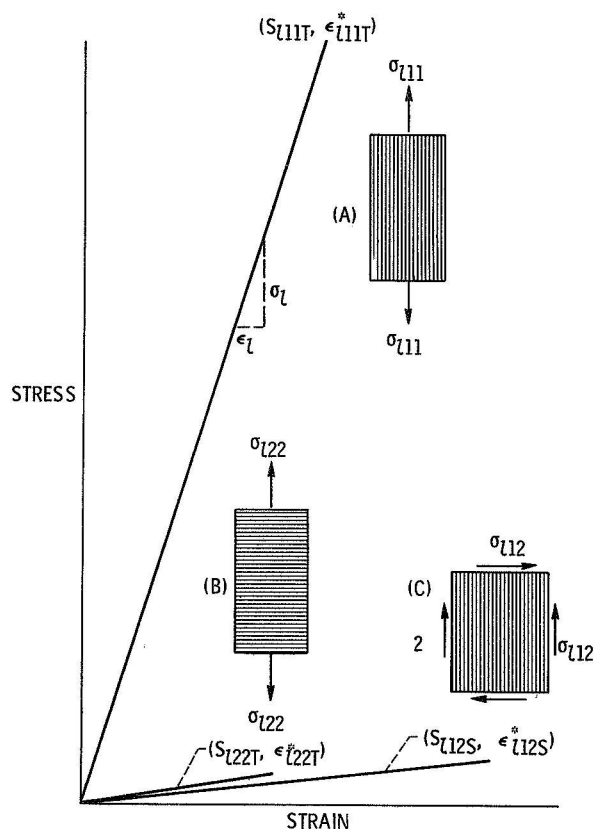


Figure 1. - Typical stress-strain curves of unidirectional fiber composite material subjected to high rate of loading.

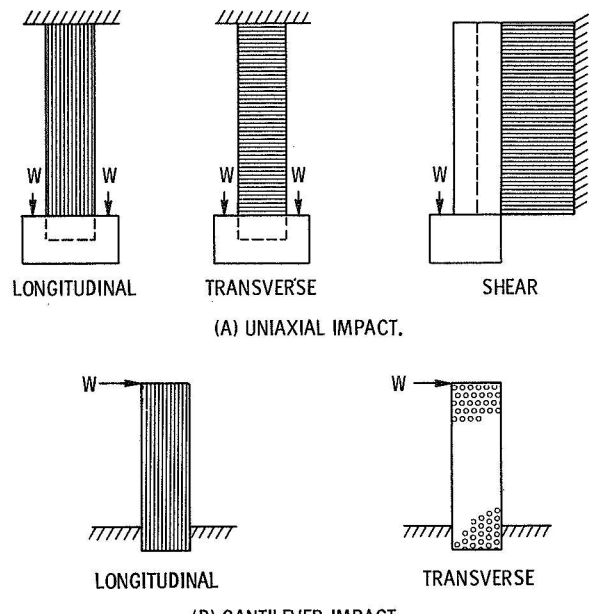


Figure 2. - Composite geometry and impact loadings.

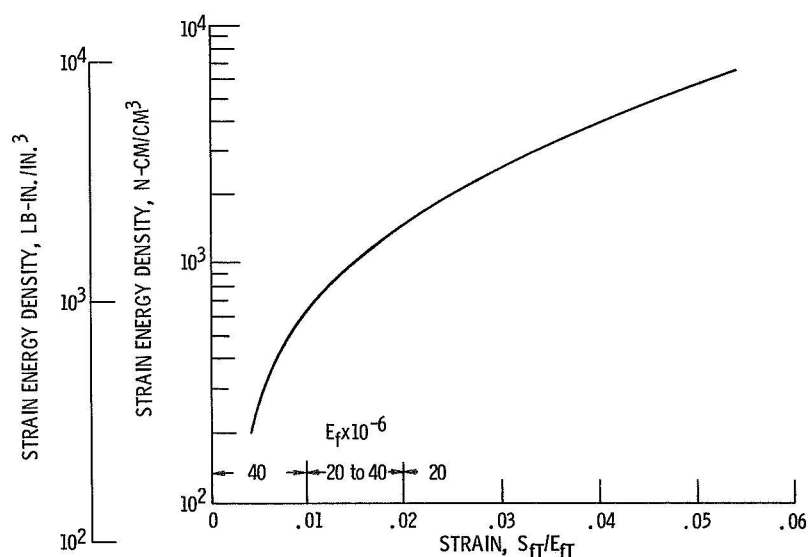


Figure 3. - Potential impact resistance of fiber composite materials from table I.

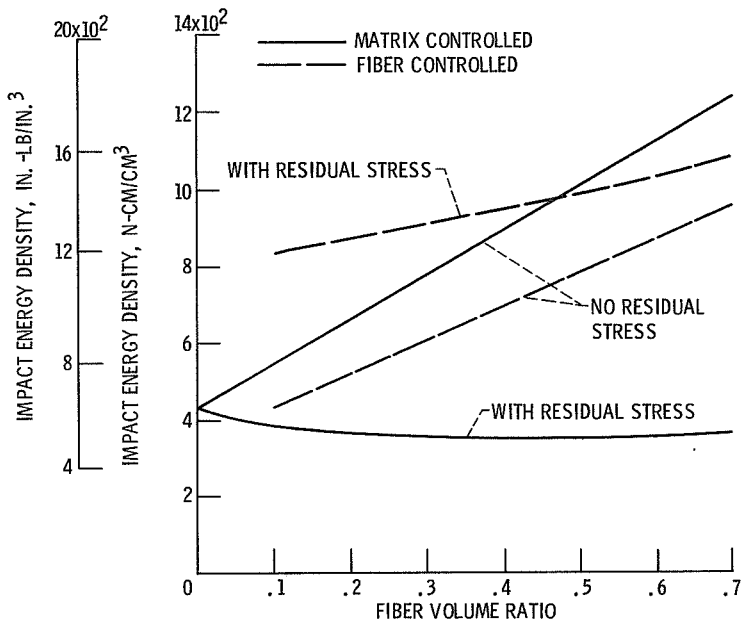


Figure 4. - Theoretical longitudinal impact resistance of (boron-silicon carbide/titanium unidirectional composite) processing temperature, 1500° F.

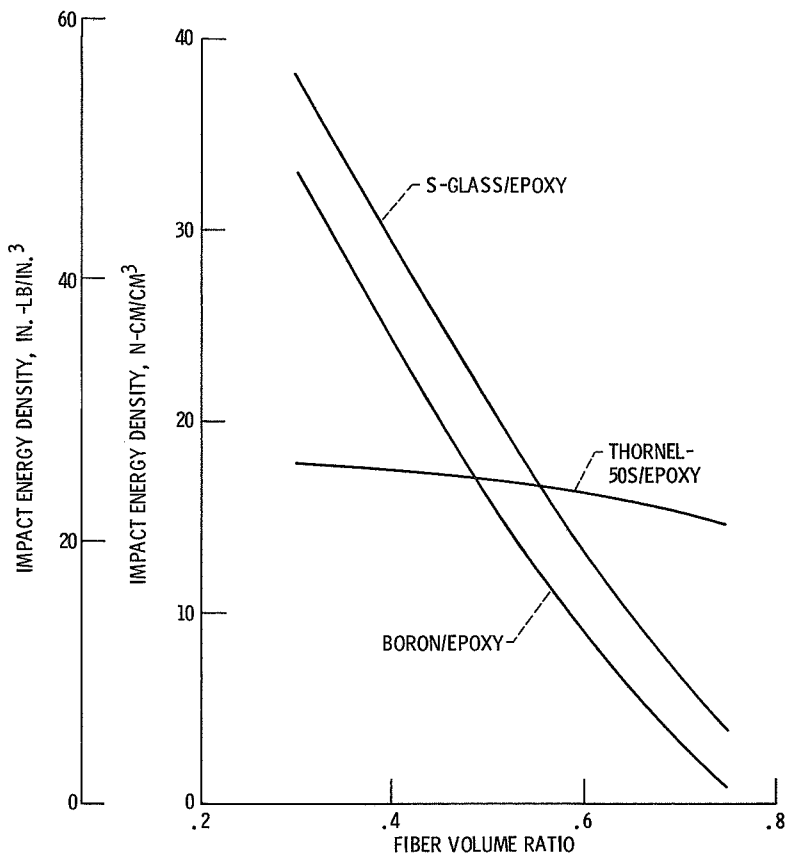


Figure 5. - Theoretical transverse impact resistance of unidirectional composites.

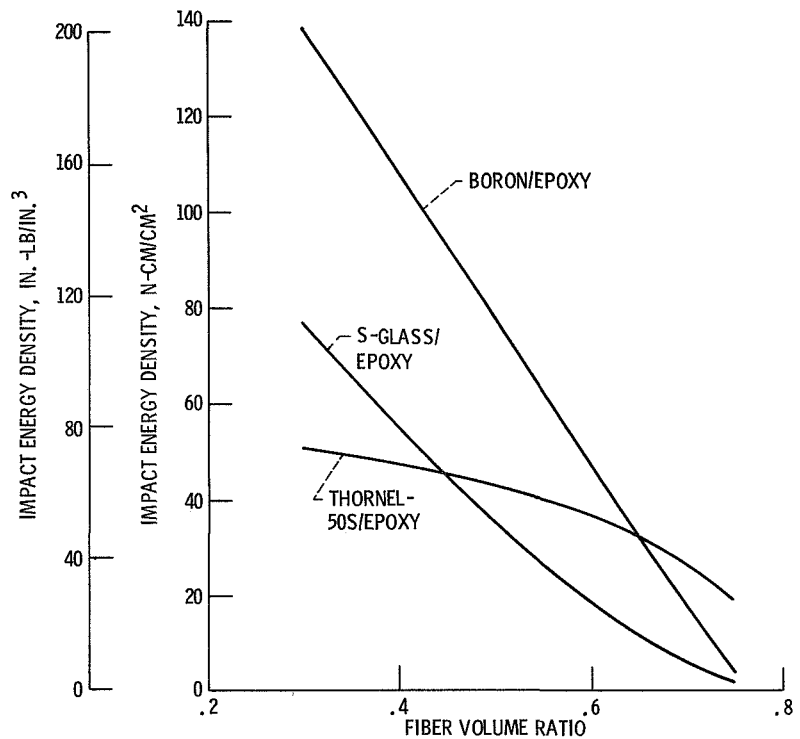


Figure 6. - Theoretical shear impact resistance of unidirectional composites.

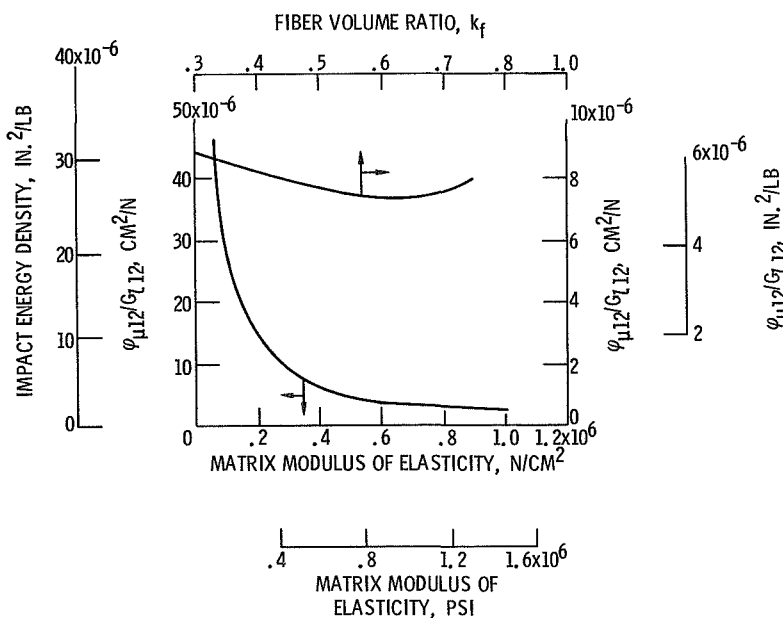


Figure 7. - Debonding parameter for Modmor-I/epoxy composite with zero voids.

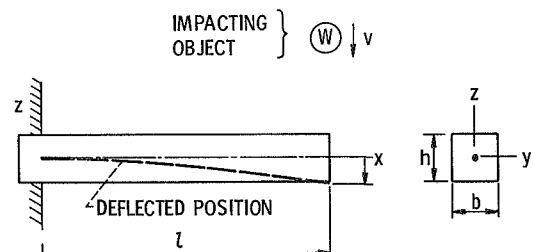


Figure 8. - Cantilever subjected to impact.

E-6254

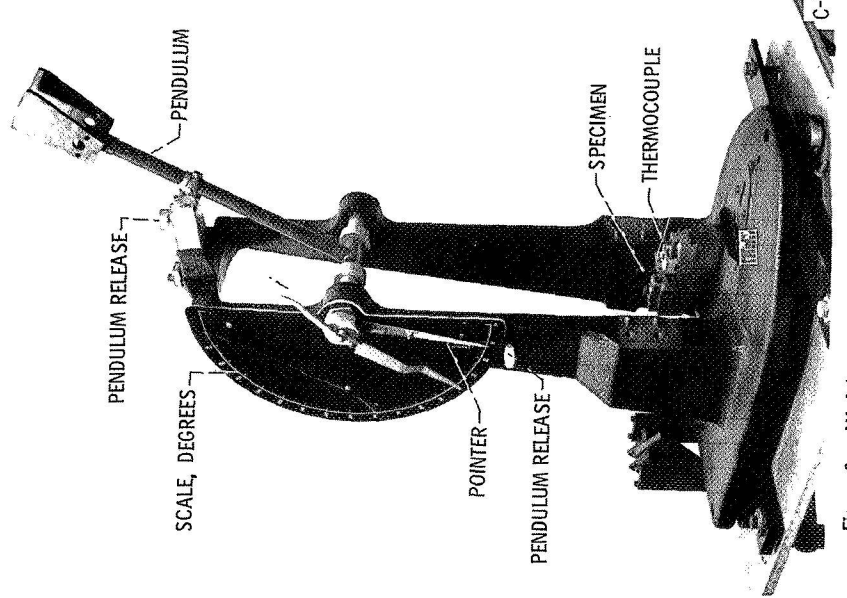


Figure 9. - Miniature-Izod pendulum-impact testing machine.

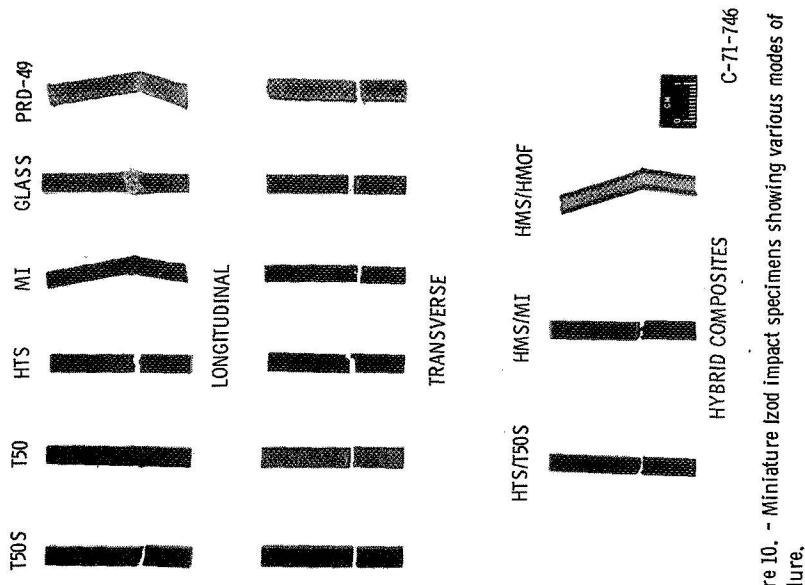


Figure 10. - Miniature Izod impact specimens showing various modes of failure.

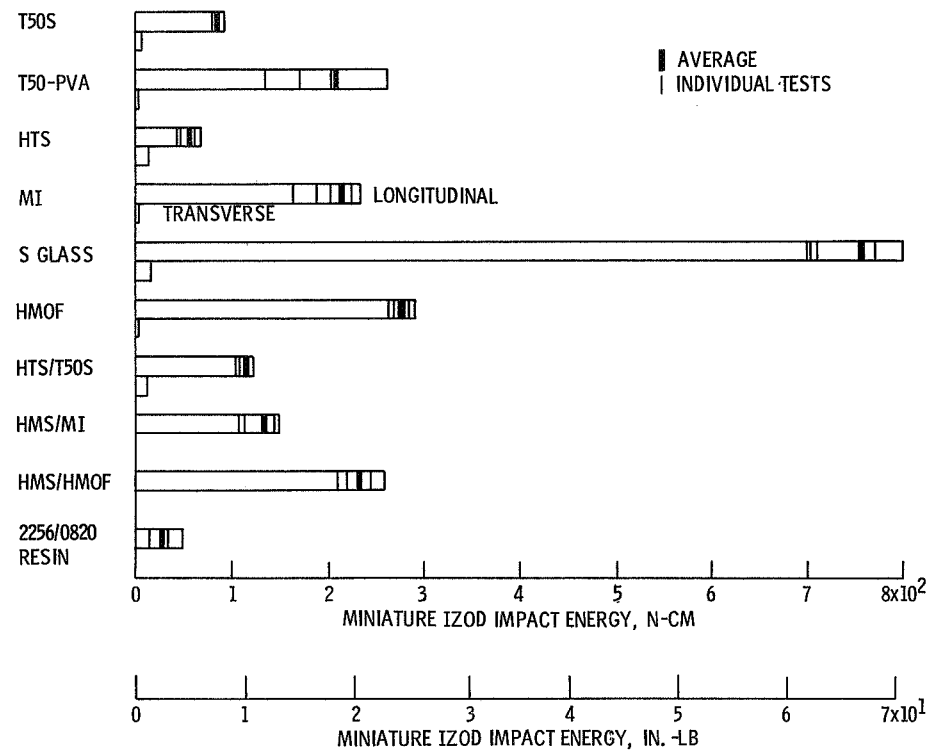


Figure 11. - Miniature Izod impact energy of fiber/ERL 2256-22L0820 composite.

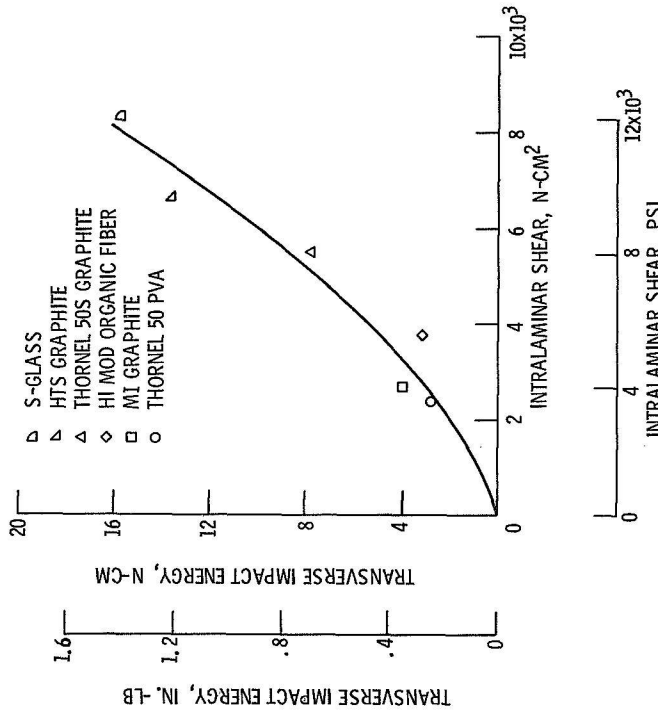


Figure 13. - Experimental results of transverse impact energy as a function of intralaminar shear for various fiber/resin composites.

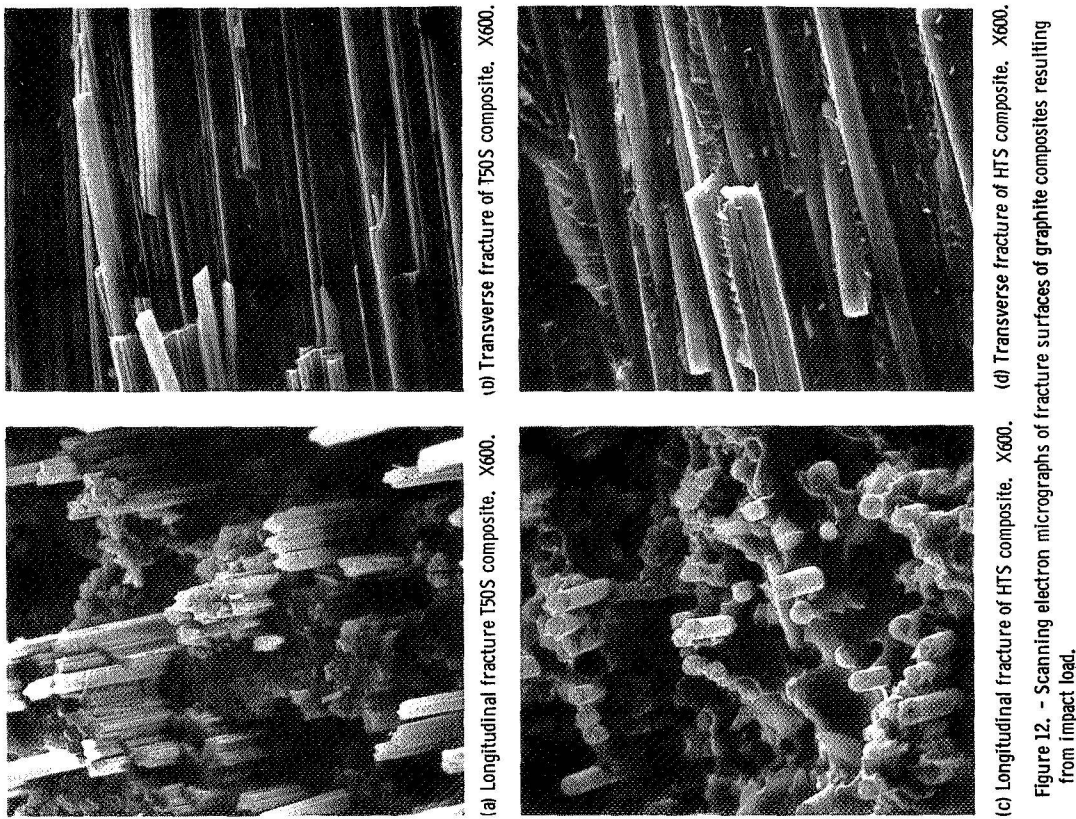


Figure 12. - Scanning electron micrographs of fracture surfaces of graphite composites resulting from impact load.